Supporting Information

Diphenanthroline Electron Transport Materials for Efficient Charge Generation Unit in Tandem Organic Light Emitting Diodes

Gyeong Woo Kim,[†] Young Hoon Son,[†] Hye In Yang,[†] Ik Jang Ko,[†] Jin Hwan Park,[†] Raju Lampande,[†] Jeonghun Sakong,[‡] Min-Jae Maeng,[‡] Jong-Am Hong,[‡] Ju Young Lee,*[,†] Yongsup Park*[,‡] and Jang Hyuk Kwon*[,†]

[†]Department of Information Display, Kyung Hee University, Hoegi-dong, Dongdaemun-gu, Seoul 130-701, Republic of Korea.

[‡]Department of Physics and Research Institute for Basic Sciences, Kyung Hee University, Hoegi-dong, Dongdaemun-gu, Seoul 130-701, Republic of Korea.

** E-mail: juyoung105@naver.com (Ju Young Lee)*
** E-mail: parky@khu.ac.kr (Yongsup Park)*
** E-mail: jhkwon@khu.ac.kr (Jang Hyuk Kwon)*

KEYWORDS: tandem OLED, charge generation unit, electron-transporting material, electron mobility, n-doping

EXPERIMENTAL SECTION

General procedures.

All reagents and solvents were purchased from commercial suppliers, Aldrich and TCI Chemical Co. To clarify molecular structures of the synthesized ETL materials, 1H- and 13C-NMR spectra were measured using Bruker Avance 400 NMR spectrometer. High-resolution mass spectra were obtained by using JEOL JMS-600W Gas Chromatography-Mass spectrometer. UV-vis absorption and PL spectra were measured using SCINCO S-4100 and JASCO FP-8500 spectrometer, respectively. Cyclic voltammetry (CV) measurements were performed by using electrochemical analysis instrument (BASi, Epsilon EC). Platinum and carbon wires were used as counter and working electrodes, respectively. An Ag wire in 0.1M $AgNO_3$ solution was incorporated as a reference electrode. Tetrabutylammonium perchlorate and ferrocenium/ferrocene (Fe+/Fe) were applied as supporting electrolyte and standard material, respectively. The potential values were transformed to the saturated calomel electrode scale using an internal standard.

Synthesis procedures

Synthesis of 2-phenyl-1,10-phenanthrolin-4-ol

A mixture of 8-aminoquinoline (13.00 g, 69.4 mmol) and ethyl acetoacetate (12.5 mL, 69.4 mmol) were stirred at 100° C for 24 hours in the presence of a catalytic amount of 1N HCl (11 drops). The reaction mixture was allowed to cool down at room temperature and then toluene (20 mL) was added, which was later removed under reduced pressure. The same process of dilution with toluene and solvent removal was repeated three times. The formed dark oily crude enamine was dissolved in diphenyl ether (20 mL) and enamine solution was slowly added to the diphenyl ether (70 mL) at 260 °C over a period of 15 minutes. After 30 minutes, the reaction mixture was cooled down to room temperature and poured into hexane. Then the solvent was decanted and the residue was recrystallized from methylene chloride and ethyl acetate to yield a light brown solid (7.3 g, 30%).

^{1}H NMR ($CDCl_3$, 400 MHz): δ [ppm] 8.96 (dd, J = 4.4, 1.6 Hz, 1H), 8.44 (d, J = 9.2 Hz, 1H), 8.32 (dd, J = 8.4, 1.6 Hz, 1H), 7.86-7.88 (m, 2H), 7.71 (d, J = 9.2 Hz, 1H), 7.67 (dd, J = 8.4, 4.4 Hz, 1H), 7.61-7.65 (m, 3H), 6.99 (s, 1H).

Synthesis of 4-chloro-2-phenyl-1,10-phenanthroline

2-phenyl-1,10-phenanthrolin-4-ol (3.4 g, 12.5 mmol) was slowly added to the phosphorus oxychloride (30 mL) and the mixture was refluxed for 4 hours. The reaction mixture was allowed to cool down to room temperature and the solvent was removed under reduced pressure. The obtained solid was treated with methylene chloride and saturated $NaHCO_3$ and separated organic layer. The aqueous layer was further extracted with methylene chloride and the combined organic layers were washed with brine, dried ($MgSO_4$), filtered and concentrated. The residue was recrystallized from methylene chloride and ethyl acetate to yield a light brown solid (2.9 g, 80%).
^{1}H NMR ($CDCl_3$, 400 MHz): δ [ppm] 9.97 (dd, J = 4.4, 1.6 Hz, 1H), 9.01 (d, J = 7.6 Hz, 1H), 8.91 (d, J = 7.2 Hz, 2H), 8.54 (d, J = 9.2 Hz, 1H), 8.46 (s, 1H), 8.24 (m, 1H), 8.10 (d, J = 9.2 Hz, 1H), 7.69 (m, 2H), 7.60 (d, J = 7.2 Hz, 1H).

Synthesis of 1,4-bis(2-phenyl-1,10-phenanthrolin-4-yl)benzene (p-bPPhenB)

A procedure similar to that used for 1,3-bis(2-phenyl-1,10-phenanthrolin-4-yl)benzene was followed but with 1,4-bis(4,4,5,5-tetramethyl-1,3,2-dioxaborolan-2-yl)benzene (1.8 g, 5.5 mmol) instead of 1,3-bis(4,4,5,5-tetramethyl-1,3,2-dioxaborolan-2-yl)benzene. The title compound was obtained as a pale brown solid (3.1 g, 96%).
^{1}H NMR ($CDCl_3$, 400 MHz): δ [ppm] 9.33 (dd, J = 4.4, 1.6 Hz, 2H), 8.45 (d, J = 7.6 Hz, 4H), 8.33 (dd, J = 8.0, 1.6 Hz, 2H), 8.21 (s, 2H), 8.10 (d, J = 9.2 Hz, 2H), 7.87 (s, 4H), 7.83 (d, J = 9.2 Hz, 2H), 7.72 (dd, J = 8.0, 4.4 Hz, 2H), 7.61 (t, J = 7.6 Hz, 4H), 7.53 (t, J = 7.6 Hz, 2H). ^{13}C NMR ($CDCl_3$, 125 MHz): δ [ppm] 157.1, 150.6, 148.6, 146.8, 139.5, 138.8, 136.1, 130.1, 129.5, 128.9, 128.6, 128.1, 126.3, 125.7, 124.1, 123.2, 121.3. HRMS (FAB+) m/z: $[M + H]^+$ calcd for $C_{42}H_{26}N_4$, 587.2236; found 587.2238.

Synthesis of 1,3-bis(2-phenyl-1,10-phenanthrolin-4-yl)benzene (m-bPPhenB)

$Pd(PPh_3)_4$ (556 mg, 0.48 mmol) was added to ~~a~~ mixture of 4-chloro-2-phenyl-1,10-phenanthroline (2.8 g, 9.6 mmol), 1,3-bis(4,4,5,5-tetramethyl-1,3,2-dioxaborolan-2-yl)benzene (1.4 g, 4.3 mmol) and Na_2CO_3 (3.1 g, 28.9 mmol) in toluene/EtOH/H_2O (75/25/50 mL) and the mixture was refluxed for 20 h under nitrogen. Then the mixture was cooled down to room temperature and extracted with ethyl acetate. The aqueous layer was further extracted with methylene chloride and the combined organic layers were washed with brine, dried ($MgSO_4$), filtered and concentrated. The residue was recrystallized from methylene chloride and methyl alcohol to yield a white solid (2.0 g, 79%).
^{1}H NMR ($CDCl_3$, 400 MHz): δ [ppm] 9.30 (dd, J = 4.4, 1.6 Hz, 2H), 8.41 (d, J = 7.6 Hz, 4H), 8.29 (dd, J = 8.0, 1.6 Hz, 2H), 8.18 (s, 2H), 8.06 (d, J = 9.2 Hz, 2H), 7.79-7.87 (m, 6H), 7.69 (dd, J = 8.0, 4.4 Hz, 2H), 7.56 (t, J = 7.6 Hz, 4H), 7.49 (t, J = 7.6 Hz, 2H). ^{13}C NMR ($CDCl_3$, 125 MHz): δ [ppm] 157.1, 150.5, 148.6, 146.6, 146.3, 139.4, 139.1, 136.3, 130.8, 129.9, 129.5, 129.2, 128.9, 128.8, 128.1, 126.3, 125.7, 124.0, 123.2, 121.4. HRMS (FAB+) m/z: $[M + H]^+$ calcd for $C_{42}H_{26}N_4$, 587.2236; found 587.2239.

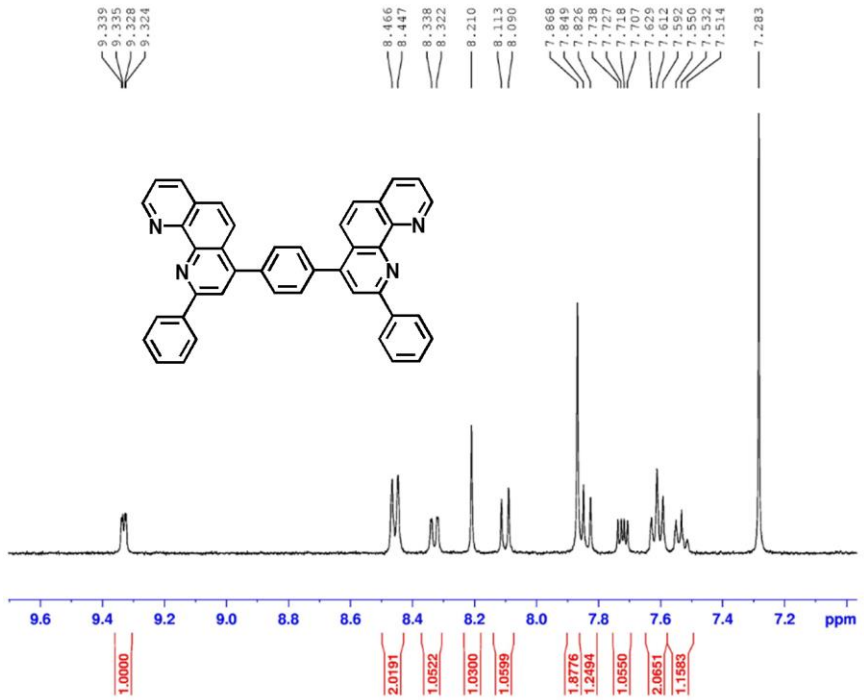

Figure S1. ^{1}H-NMR spectrum of p-bPPhenB

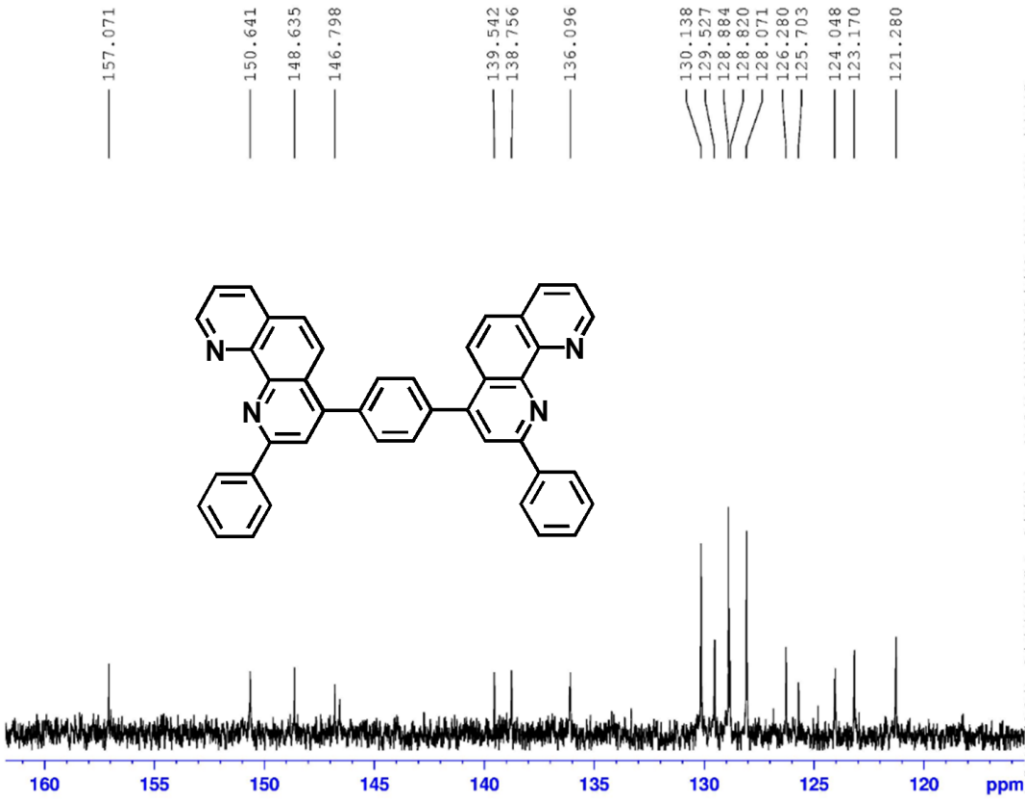

Figure S2. ^{13}C-NMR spectrum of p-bPPhenB

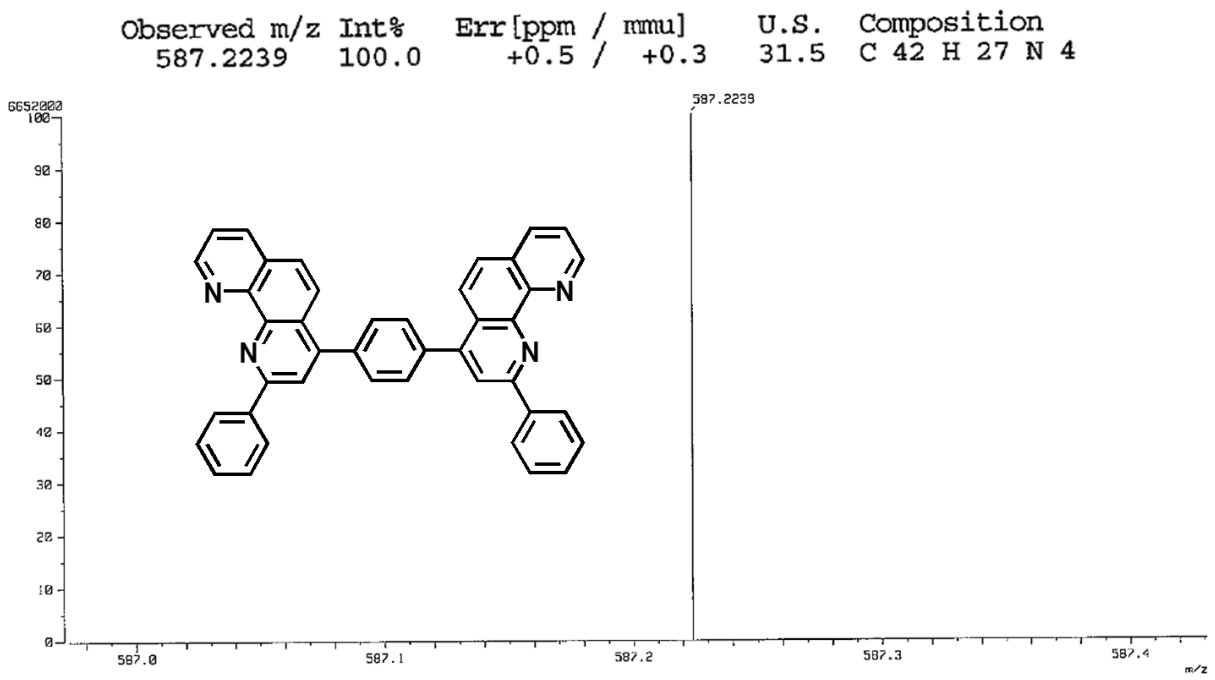

Figure S3. HRMS spectrum of p-bPPhenB

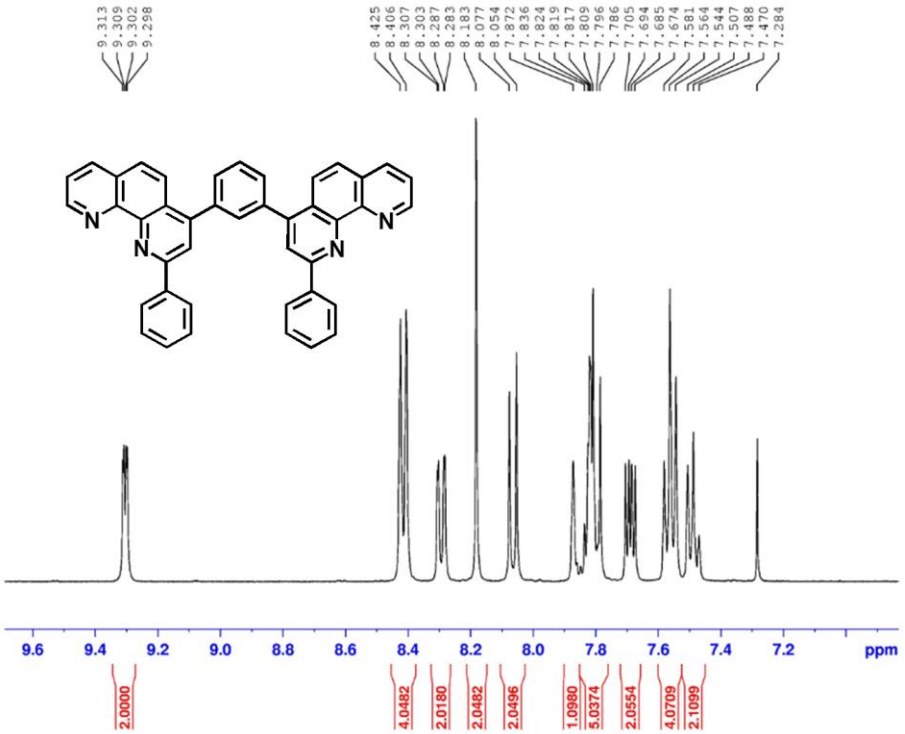

Figure S 4 ^{1}H-NMR spectrum of m-bPPhenB

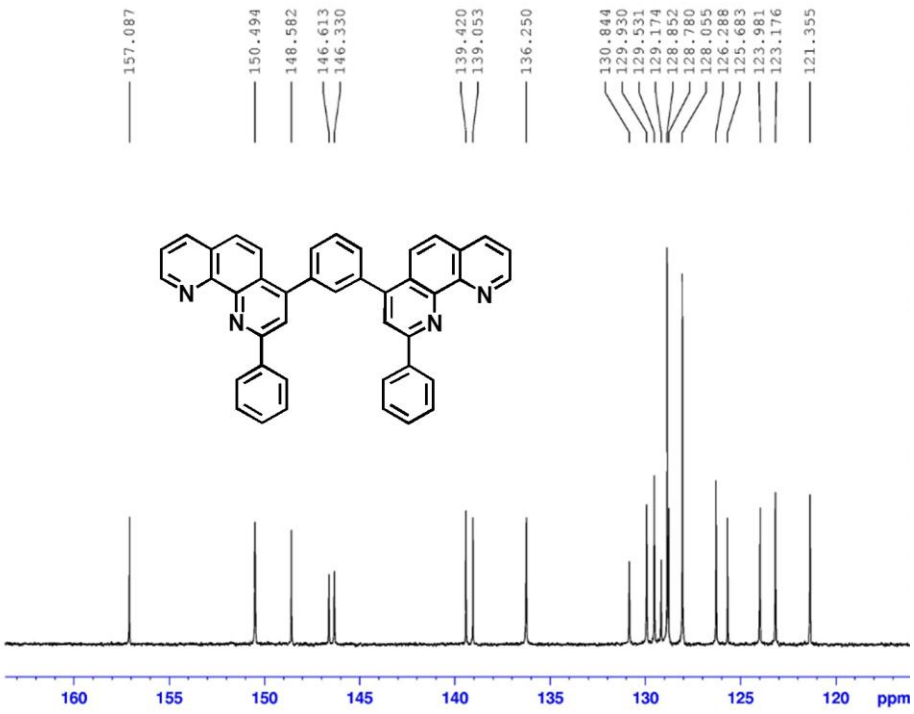

Figure S5. ^{13}C-NMR spectrum of m-bPPhenB

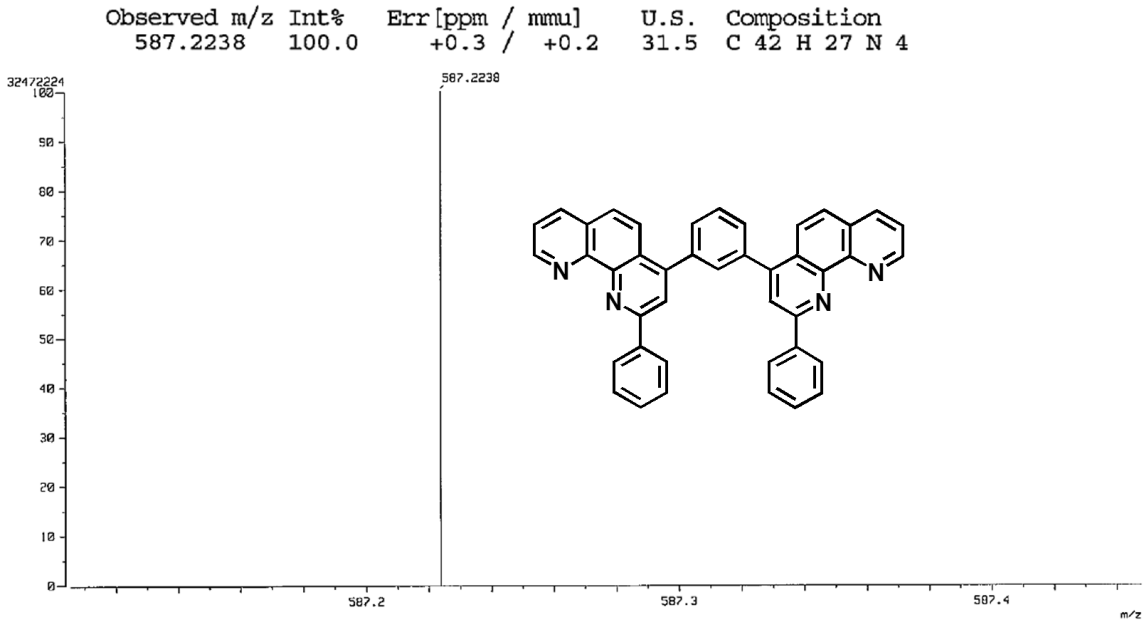

Figure S6. HRMS spectrum of m-bPPhenB

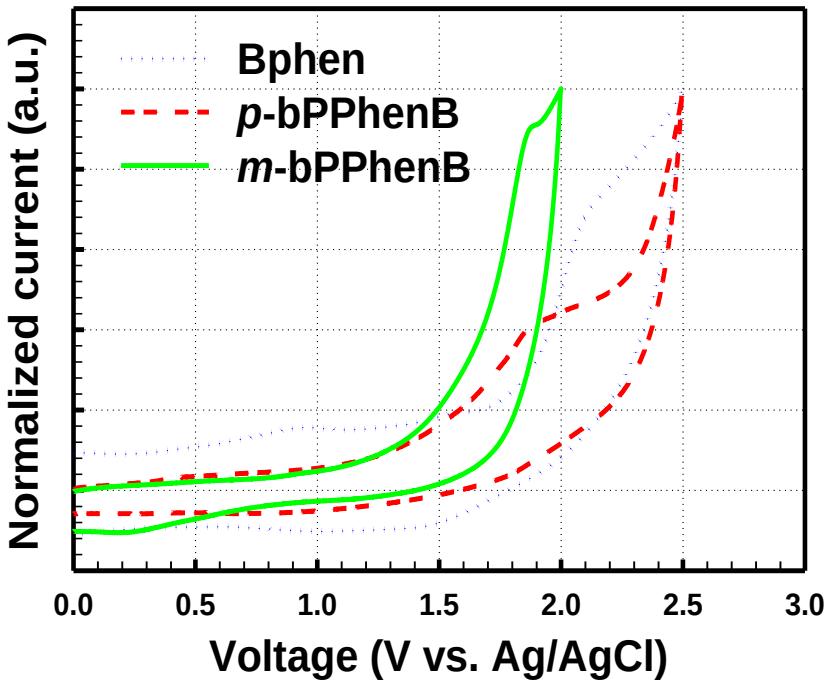

Figure S7. Cyclic voltammograms of Bphen, p-bPPhenB, and m-bPPhenB

	Molecular structure	Neutral state	Anionic state
Phen	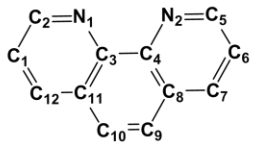	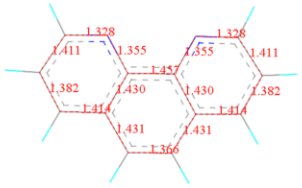	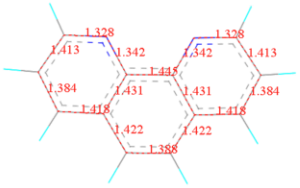
4-Pphen	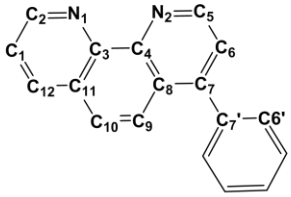	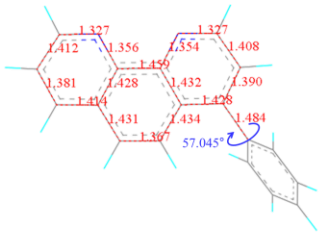	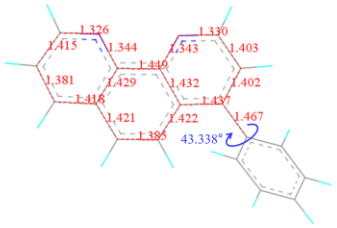
2-Pphen	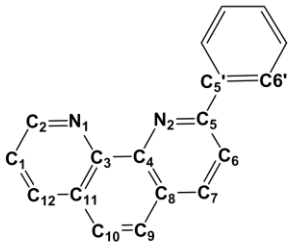	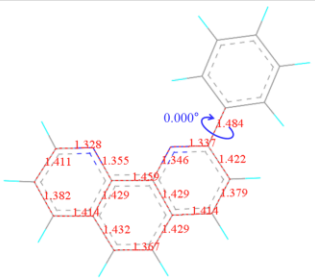	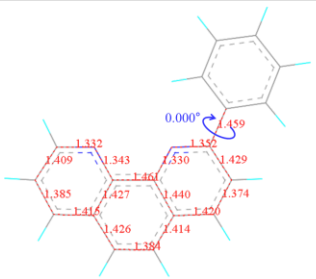
2,9-Pphen	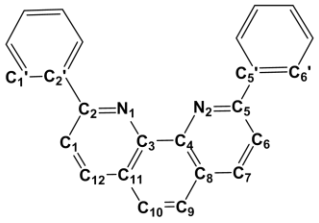	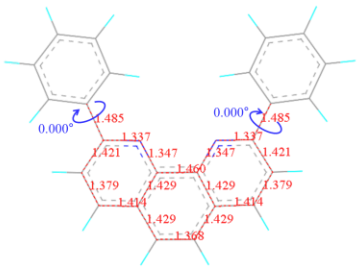	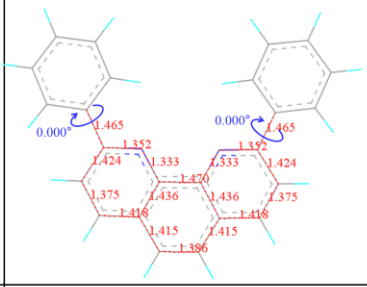
2,4-Pphen	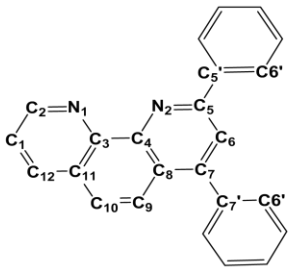	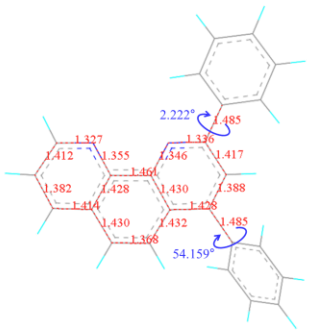	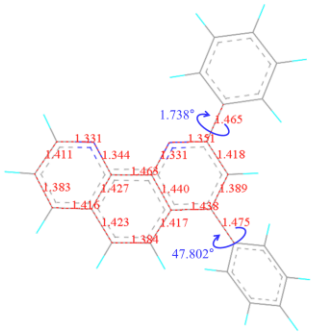
4,7-PPhen	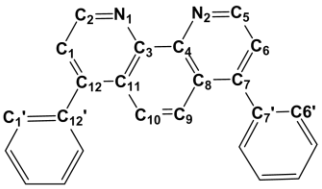	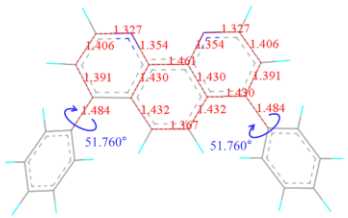	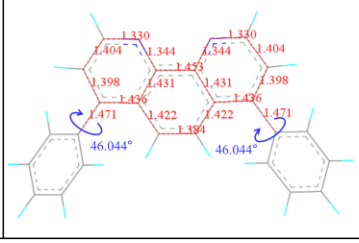

Figure S8. Optimized molecular geometries of 1,10-phenanthroline derivatives both for neutral and anionic states.

Table S1. Calculated bond lengths and torsional angles between 1,10-phenantroline and phenyl ring of 1,10-phenanthroline derivatives both for neutral and anionic states.

			Phen			4-PPhen			2-PPhen			2,9-PPhen			2,4-PPhen			4,7-PPhen		
			N[a]	A[b]	|Δ|[c]	N[a]	A[b]	|Δ|[c]	N[a]	A[b]	|Δ|[c]	N[a]	A[b]	|Δ|[c]	N[a]	A[b]	|Δ|[c]	N[a]	A[b]	|Δ|[c]
Bond length (Å)	Phenanthroline ring	C_1-C_2	1.411	1.413	**0.002**	1.412	1.415	**0.003**	1.411	1.409	**0.002**	1.421	1.424	**0.003**	1.412	1.411	**0.001**	1.406	1.403	**0.003**
		C_2-N_1	1.328	1.328	**0.000**	1.327	1.326	**0.001**	1.328	1.332	**0.004**	1.337	1.352	**0.015**	1.327	1.331	**0.004**	1.328	1.329	**0.001**
		N_1-C_3	1.355	1.342	**0.013**	1.355	1.344	**0.011**	1.355	1.343	**0.012**	1.347	1.333	**0.014**	1.355	1.344	**0.011**	1.354	1.344	**0.010**
		C_3-C_4	1.452	1.445	**0.007**	1.459	1.449	**0.01**	1.459	1.461	**0.002**	1.46	1.47	**0.01**	1.461	1.463	**0.002**	1.451	1.452	**0.001**
		C_4-N_2	1.355	1.342	**0.013**	1.354	1.343	**0.011**	1.346	1.33	**0.016**	1.347	1.333	**0.014**	1.346	1.331	**0.015**	1.354	1.344	**0.010**
		N_2-C_5	1.328	1.328	**0.000**	1.327	1.33	**0.003**	1.357	1.352	**0.005**	1.337	1.352	**0.015**	1.336	1.351	**0.015**	1.328	1.329	**0.001**
		C_5-C_6	1.411	1.413	**0.002**	1.407	1.403	**0.004**	1.422	1.429	**0.007**	1.421	1.424	**0.003**	1.417	1.418	**0.001**	1.406	1.403	**0.003**
		C_6-C_7	1.382	1.384	**0.002**	1.391	1.401	**0.01**	1.379	1.374	**0.005**	1.379	1.375	**0.004**	1.388	1.389	**0.001**	1.391	1.398	**0.007**
		C_7-C_8	1.414	1.418	**0.004**	1.429	1.437	**0.008**	1.414	1.42	**0.006**	1.414	1.418	**0.004**	1.428	1.438	**0.01**	1.429	1.436	**0.007**
		C_8-C_9	1.431	1.422	**0.009**	1.434	1.423	**0.011**	1.429	1.414	**0.015**	1.429	1.415	**0.014**	1.432	1.417	**0.015**	1.432	1.422	**0.010**
		C_9-C_{10}	1.366	1.388	**0.022**	1.366	1.384	**0.018**	1.367	1.384	**0.017**	1.368	1.386	**0.018**	1.368	1.384	**0.016**	1.367	1.384	**0.017**
		C_{10}-C_{11}	1.431	1.422	**0.009**	1.429	1.421	**0.008**	1.432	1.426	**0.006**	1.429	1.415	**0.014**	1.43	1.423	**0.007**	1.432	1.422	**0.010**
		C_{11}-C_{12}	1.414	1.418	**0.004**	1.414	1.417	**0.003**	1.414	1.415	**0.001**	1.414	1.418	**0.004**	1.414	1.416	**0.002**	1.429	1.436	**0.007**
		C_{12}-C_1	1.382	1.384	**0.002**	1.381	1.381	**0.000**	1.382	1.385	**0.003**	1.379	1.375	**0.004**	1.381	1.383	**0.002**	1.391	1.398	**0.007**
		C_3-C_{11}				1.428	1.429	**0.001**	1.429	1.427	**0.002**	1.429	1.436	**0.007**	1.428	1.427	**0.001**	1.430	1.431	**0.001**
		C_4-C_8				1.432	1.432	**0.000**	1.429	1.440	**0.011**	1.429	1.436	**0.007**	1.430	1.440	**0.010**	1.430	1.431	**0.001**
		Total			**0.089**			**0.102**			**0.114**			**0.150**			**0.113**			**0.096**
	Inter-ring distance (phenantrolin-phenyl)	C_7-C_7'				1.484	1.467	**0.017**							1.485	1.465	**0.020**	1.484	1.471	**0.013**
		C_5-C_5'							1.484	1.459	**0.025**	1.485	1.465	**0.020**	1.485	1.475	**0.010**			
		C_2-C_1'										1.485	1.465	**0.020**						
		C_{12}-C_{12}'																1.484	1.471	**0.013**
		Total						**0.017**			**0.025**			**0.040**			**0.030**			**0.026**
Torsional angle (°)	C_6-C_7-C_7'-C_6'					53.290	43.920	**9.370**							54.159	47.802	**6.357**	51.739	46.044	**5.695**
	C_6-C_5-C_5'-C_6'								0.000	0.000	**0.000**	0.000	0.000	**0.000**	2.222	1.738	**0.484**			
	C_1-C_2-C_2'-C_1'											0.000	0.000	**0.000**						
	C_1-C_{12}-C_{12}'-C_1'																	51.739	46.044	**5.695**
	Total							**9.370**			**0.000**			**0.000**			**6.841**			**11.390**

[a] Neutral state, [b] Anionic state, [c] Absolute value of difference between neutral and anionic state.

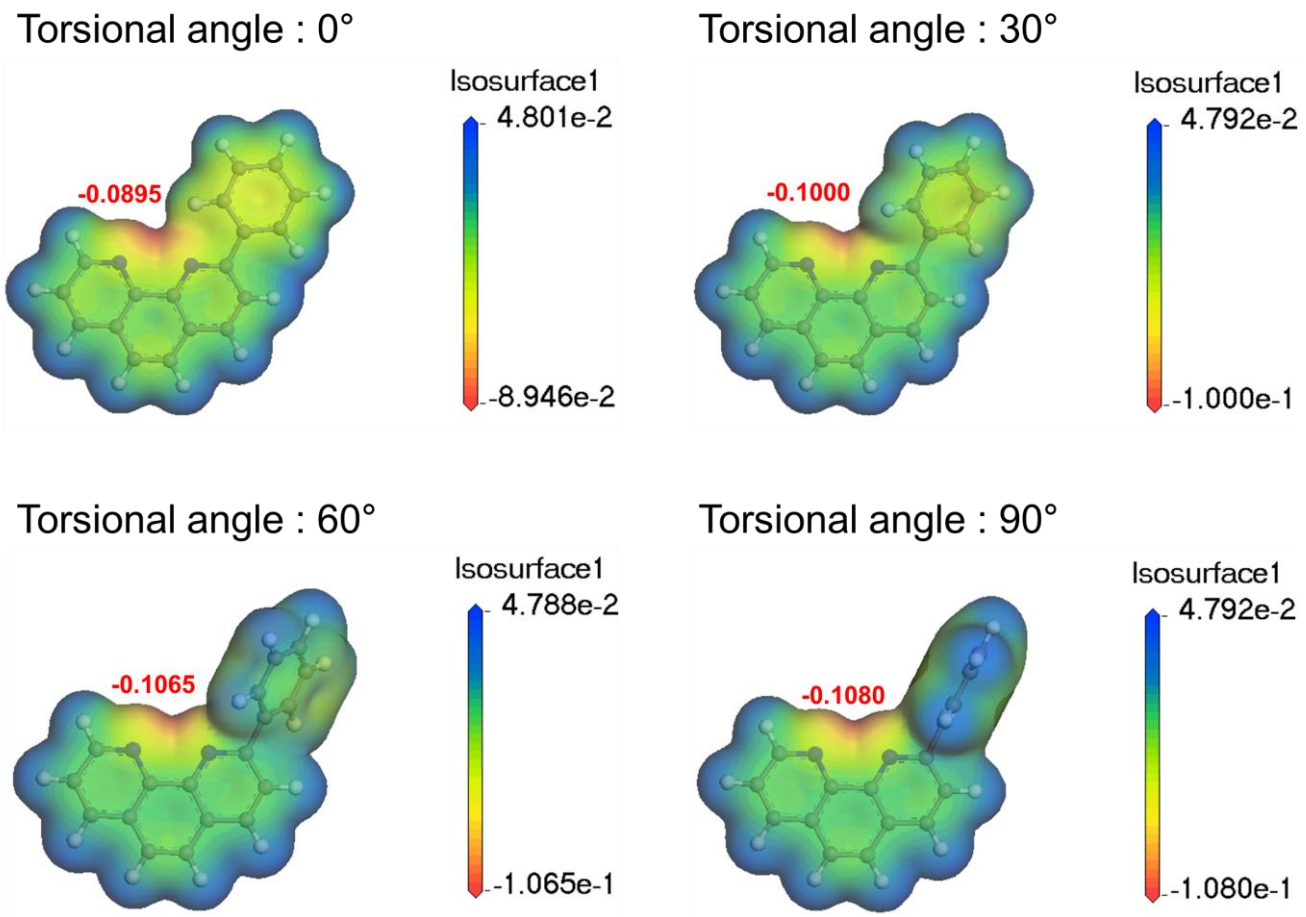

Figure S9. Comparison of negative ESP values of 2-PPhen with different torsional angle between Phen and phenyl.

	Molecular structure	Neutral state	Anionic state
p-bPPhenB	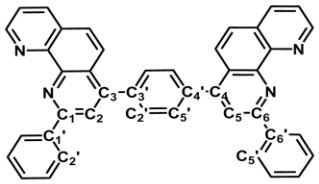	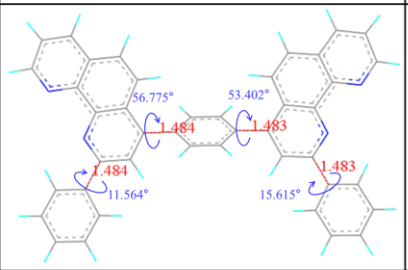	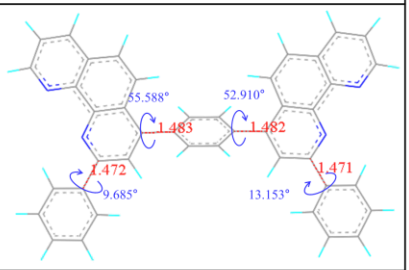
m-bPPhenB	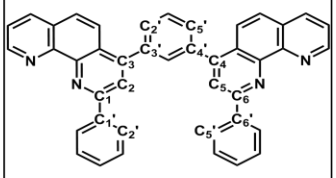	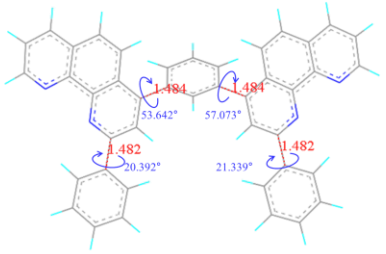	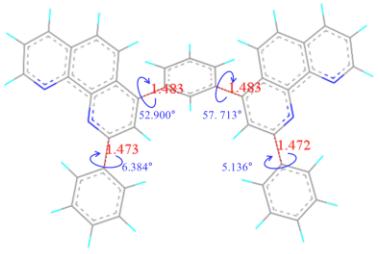

Figure S10 .Optimized molecular geometries of p-bPPhenB and m-bPPhenB both for neutral and anionic states.

Table S2. Calculated bond lengths (inter-ring distances) and torsional angles between 1,10 phenantroline and phenyl ring of p-bPPhenB and m-bPPhenB both for neutral and anionic states.

		p-bPPhenB			m-bPPhenB		
		N[a]	A[b]	|Δ|[c]	N[a]	A[b]	|Δ|[c]
Bond length (inter-ring distance) (Å)	C_1-C_1'	1.484	1.472	**0.012**	1.482	1.473	**0.009**
	C_3-C_3'	1.484	1.483	**0.001**	1.484	1.483	**0.001**
	C_4-C_4'	1.483	1.482	**0.001**	1.484	1.483	**0.001**
	C_6-C_6'	1.483	1.471	**0.012**	1.482	1.472	**0.01**
	Total			**0.026**			**0.021**
Torsional angle (°)	C_2-C_1-C_1'-C_2'	11.564	9.685	**1.879**	20.392	6.384	**14.008**
	C_2-C_3-C_3'-C_2'	56.775	55.588	**1.187**	53.642	52.900	**0.742**
	C_5-C_4-C_4'-C_5'	53.402	52.91	**0.492**	57.073	57.371	**0.298**
	C_5-C_6-C_6'-C_5'	15.615	13.153	**2.462**	21.339	5.436	**15.903**
	Total			**6.020**			**30.951**

[a] Neutral state, [b] Anionic state, [c] Absolute value of difference between neutral and anionic state.

DEVICE FABRICATION AND CHARACTERIZATION

Fabrication of EOD, CGU, single and tandem PhOLED devices. All the organic and inorganic materials such as 1,4,5,8,9,11-hexaazatriphenylene hexacarbonitrile (HATCN), 1,1-bis-(4-bis(4-methyl-phenyl)-amino-phenyl)-cyclohexane (TAPC), bis(10-hydroxybenzo[h]quinolinato)beryllium ($Bebq_2$), Iridium(III) bis(4-methyl-2-(3,5-dimethylphenyl)quinolinato-*N*,C2′) tetramethylheptadionate (Ir(mphmq)2(tmd)), 1,3,5-tri(m-pyrid-3-yl-phenyl)benzene (TmPyPB), 4,7-diphenyl-1,10-phenanthroline (Bphen), lithium (Li), and aluminium (Al) were purchased from Luminescence Technology Corporation and Sigma-Aldrich.

To fabricate single and tandem red PhOLEDs, commercially available patterned ITO substrates were utilized. All organic and inorganic layers were thermally evaporated on the pre-cleaned ITO substrates in a high vacuum chamber at base pressure of 10^{-7} Torr. Finally all devices were encapsulated using glass cover and UV-cured resin in nitrogen atmosphere.

Characterization of EOD, CGU, single and tandem PhOLED devices

Current density-voltage (J-V) curves of EOD, CGU, single and tandem red PhOLED devices were obtained by using Keithley 2635A Source Meter Unit (SMU). EL characteristics including luminance voltage (L-V) curve, EQE, power efficiency, EL spectrum, and CIE color coordinates of the red OLED devices were measured by using SMU with Konica Minolta CS-100A and CS-2000 spectroradiometer. All the measurements were performed in ambient condition.

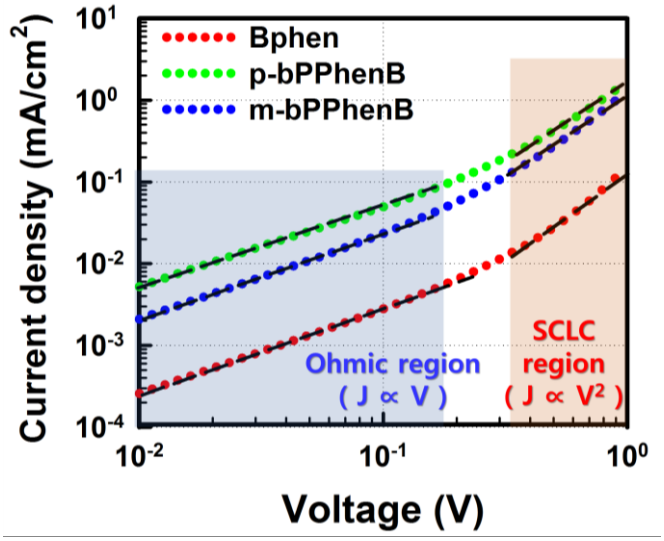

Figure S11. Current density – voltage characteristics of EODs

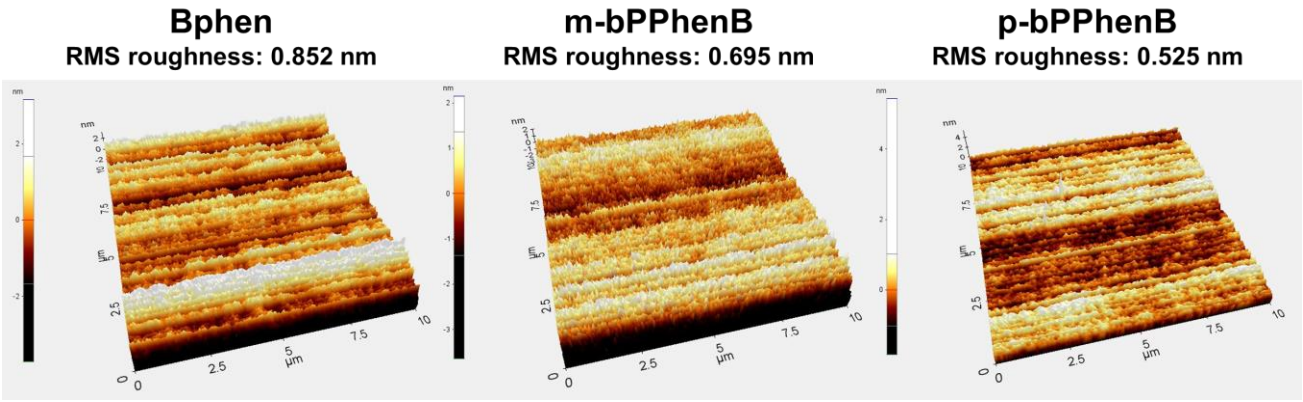

Figure S12. AFM images of 100 nm-thick Bphen, m-bPPhenB and p-bPPhenB film.

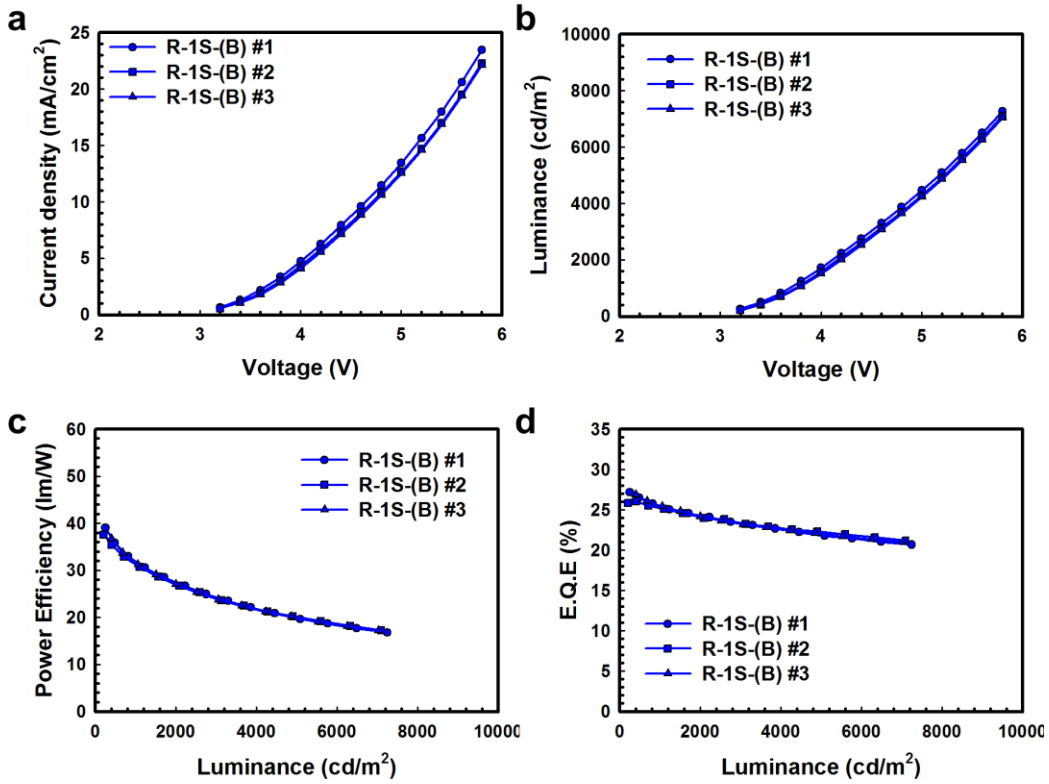

Figure S13. Current density-voltage (a) and Luminance-voltage (b) characteristics, power efficiencies (c), and external quantum efficiencies of single-stack red PhOLEDs using Bphen (R-1S-(B)).

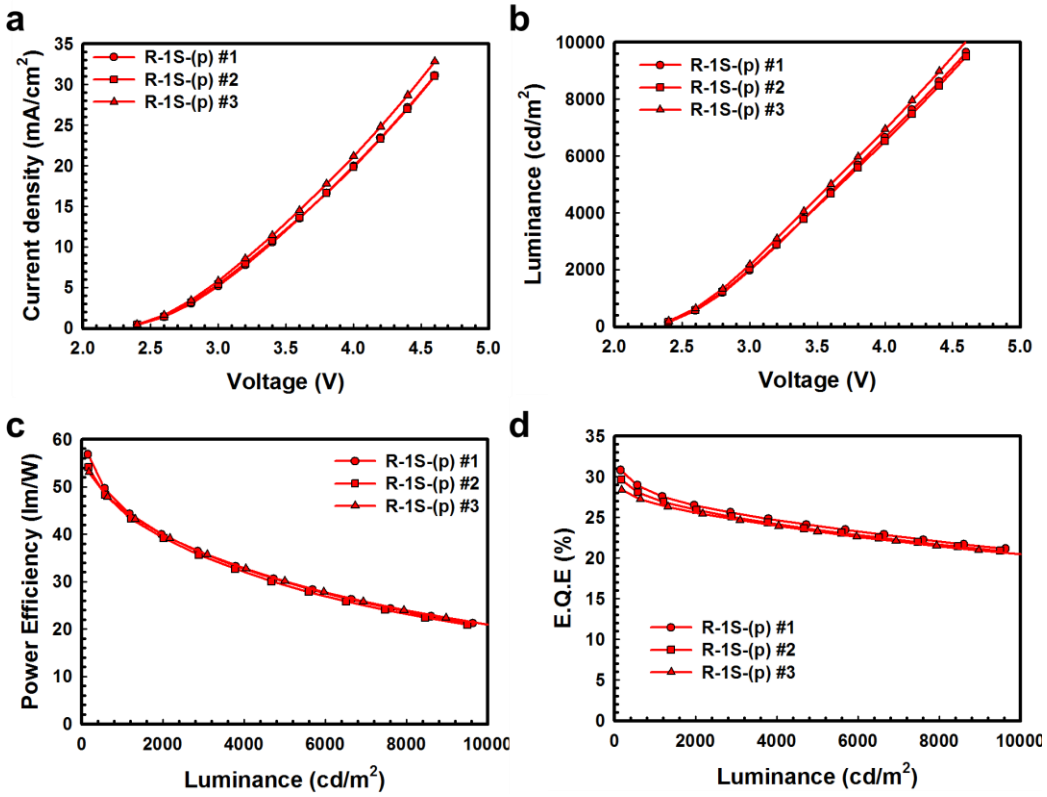

Figure S14. Current density-voltage (a) and Luminance-voltage (b) characteristics, power efficiencies (c), and external quantum efficiencies of single-stack red PhOLEDs using p-bPPhenB (R-1S-(p)).

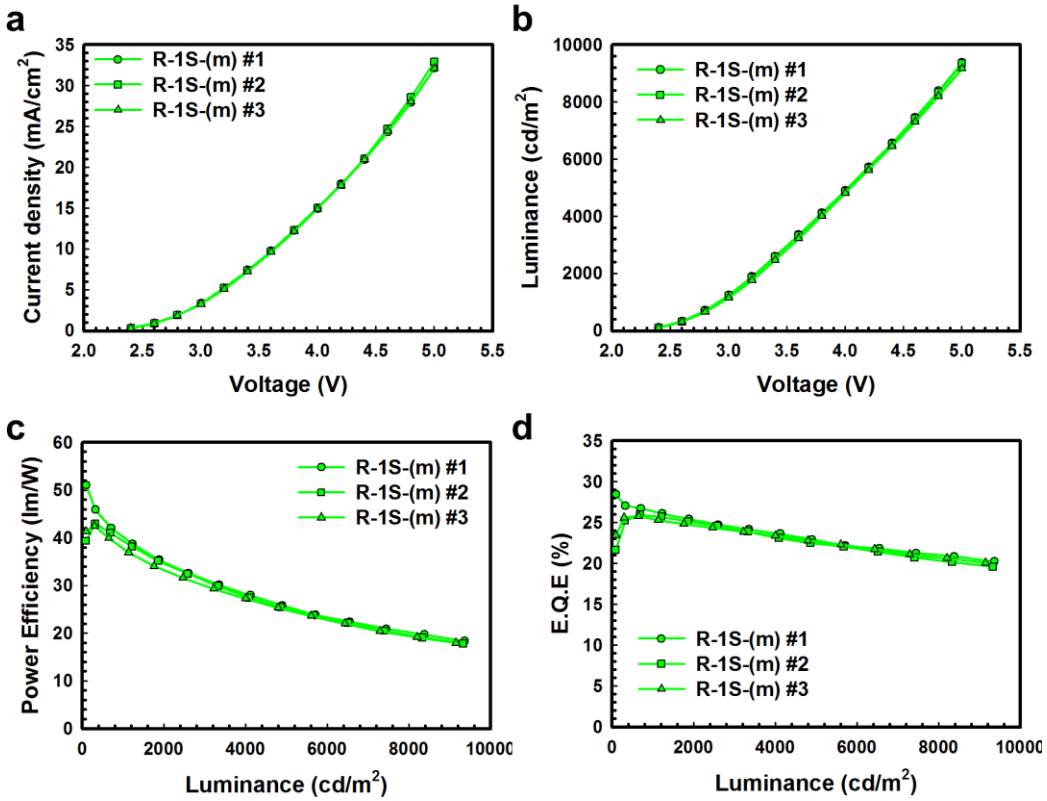

Figure S15. Current density-voltage (a) and Luminance-voltage (b) characteristics, power efficiencies (c), and external quantum efficiencies of single-stack red PhOLEDs using m-bPPhenB (R-1S-(m)).

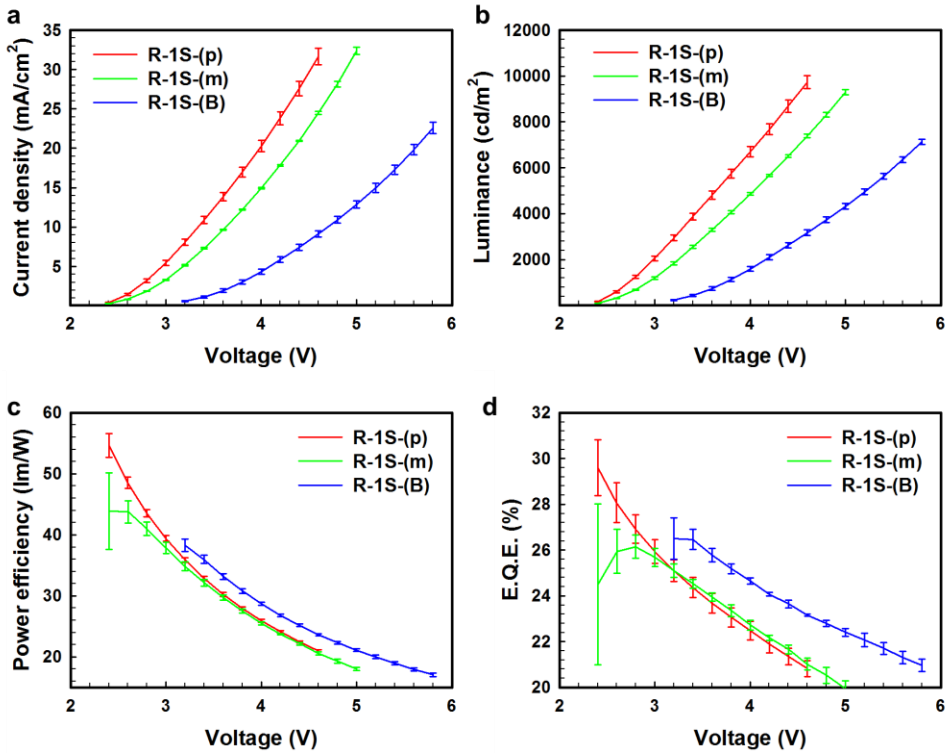

Figure S16. Current density (a), luminance (b), power efficiency (c) and E.Q.E. (d) versus voltage for single-stack red PhOLEDs using p-bPPhenB, m-bPPhenB and Bphen. Standard deviations are displayed with error bars.

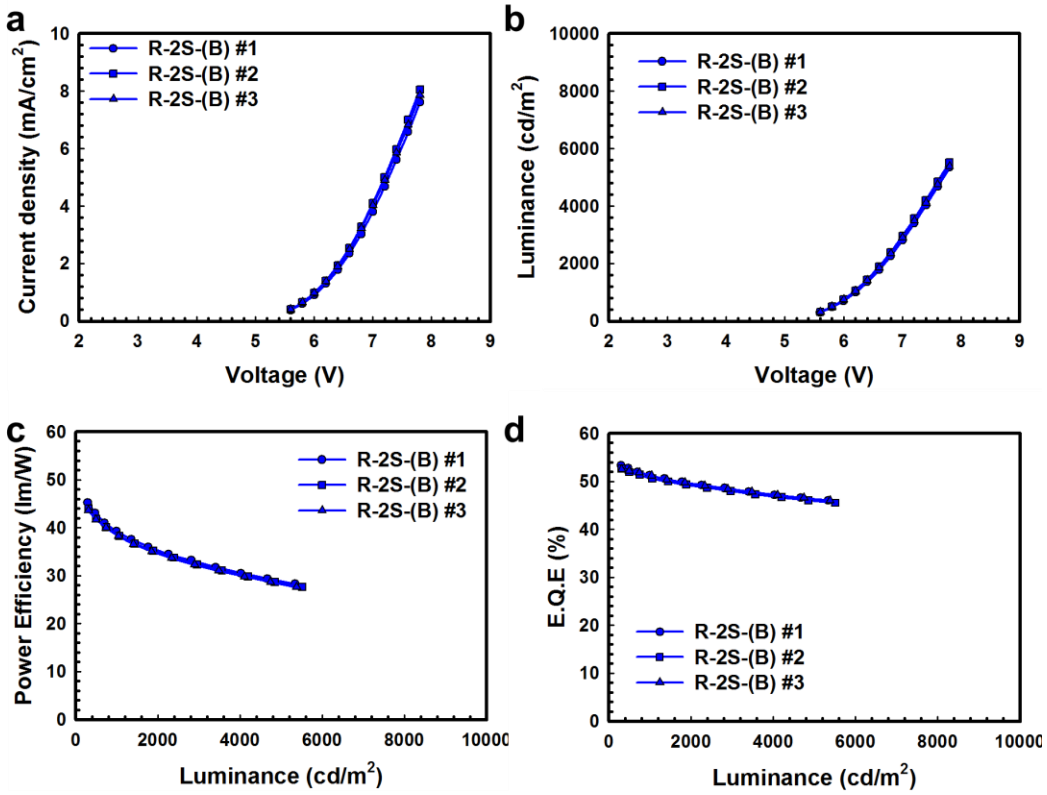

Figure S17. Current density-voltage (a) and Luminance-voltage (b) characteristics, power efficiencies (c), and external quantum efficiencies of two-stack red PhOLEDs using Bphen (R-2S-(B)).

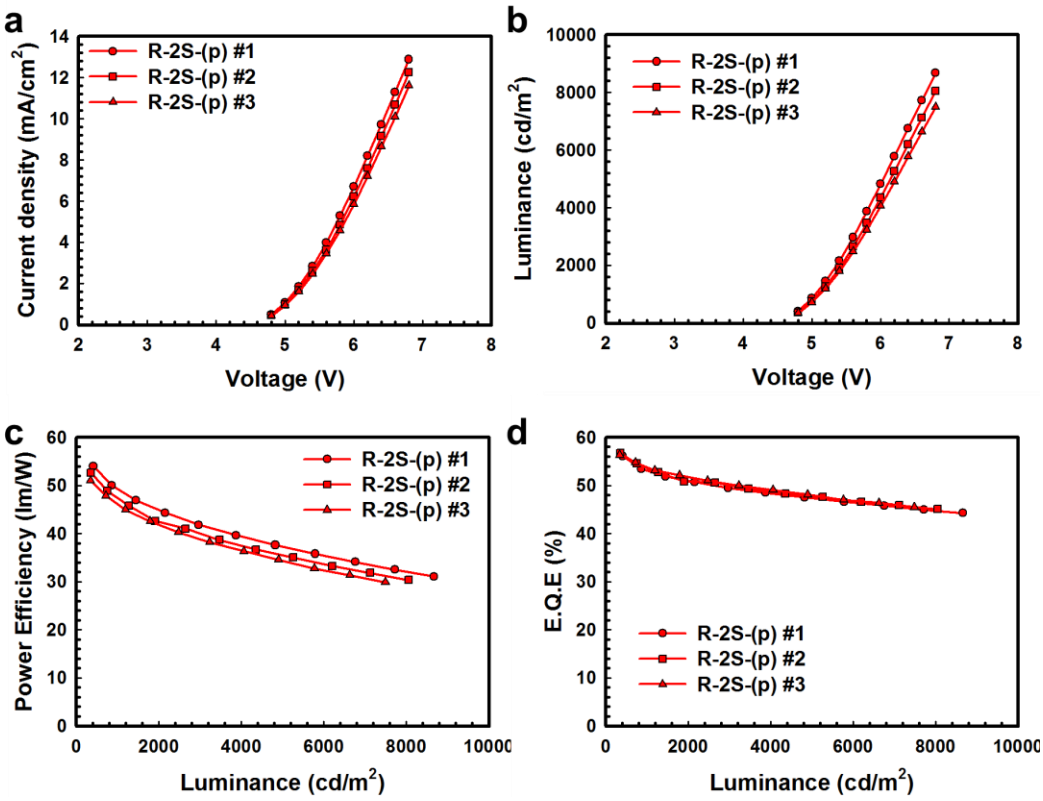

Figure S18. Current density-voltage (a) and Luminance-voltage (b) characteristics, power efficiencies (c), and external quantum efficiencies of two-stack red PhOLEDs using p-bPPhenB (R-2S-(p)).

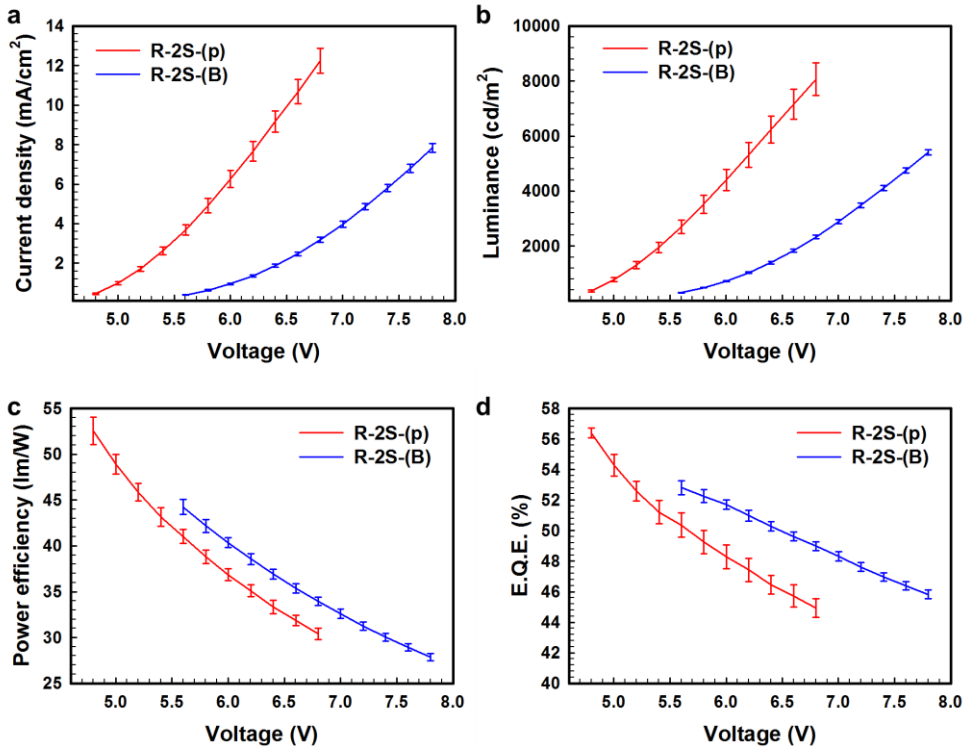

Figure S19. Current density (a), luminance (b), power efficiency (c) and E.Q.E. (d) versus voltage for two-stack red PhOLEDs using p-bPPhenB, m-bPPhenB and Bphen. Standard deviations are displayed with error bars.

Table S3. Electroluminescence performances of all the fabricated single- and two-stack OLEDs

Devices		V_D [b] [V]	PE [lm/W]	EQE [%]
R-1S-(B)	#1	3.7	39.0 [a] / 32.0 [b]	27.1 [a] / 25.5 [b]
	#2	3.7	37.6 [a] / 31.1 [b]	26.0 [a] / 25.2 [b]
	#3	3.8	36.7 [a] / 31.2 [b]	26.9 [a] / 25.4 [b]
	Average value	3.7	37.8 [a] / 31.4 [b]	26.7 [a] / 25.4 [b]
R-1S-(p)	#1	2.7	56.8 [a] / 45.9 [b]	30.8 [a] / 28.0 [b]
	#2	2.7	54.1 [a] / 45.4 [b]	29.6 [a] / 27.2 [b]
	#3	2.7	53.1 [a] / 45.1 [b]	28.4 [a] / 26.7 [b]
	Average value	2.7	54.6 [a] / 45.5 [b]	29.6 [a] / 27.3 [b]
R-1S-(m)	#1	2.9	51.0 [a] / 40.2 [b]	28.4 [a] / 26.4 [b]
	#2	2.9	42.9 [a] / 39.4 [b]	26.0 [a] / 25.7 [b]
	#3	2.9	42.5 [a] / 37.7 [b]	25.8 [a] / 25.5 [b]
	Average value	2.9	45.5 [a] /39.1 [b]	26.7 [a] / 25.9 [b]
R-2S-(B)	#1	6.2	45.2 [a] / 39.2 [b]	53.3 [a] / 51.1 [b]
	#2	6.2	45.2 [a] / 38.2 [b]	52.6 [a] / 50.6 [b]
	#3	6.2	43.6 [a] / 38.2 [b]	52.5 [a] / 51.2 [b]
	Average value	6.2	44.7 [a] / 38.5 [b]	52.8 [a] / 51.0 [b]
R-2S-(p)	#1	5.0	54.0 [a] / 49.3 [b]	56.1 [a] / 53.1 [b]
	#2	5.1	52.6 [a] / 47.5 [b]	56.7 [a] / 53.6 [b]
	#3	5.1	51.0 [a] / 46.0 [b]	56.3 [a] / 53.2 [b]
	Average value	5.1	52.5 [a] / 47.6 [b]	56.4 [a] / 53.3 [b]

[a] Maximum value, [b] Measured value at 1,000 cd/m^2

UPS measurement. UPS measurement was carried out in an ultra-high-vacuum analysis chamber with base pressure of 1×10^{-9} Torr. Photoelectron spectra were recorded using a modified KRATOS AXIS165 system with a He I (21.2 eV) source for UPS. A sample bias of −10 V was applied when the UPS spectra were recorded to clearly distinguish the secondary electron cut-off positions. Energy resolutions were approximately 0.1 eV for UPS. Any type of temperature dependent measurements was not attempted during experiments.
The device structures for first and second experiments are as follows: TAPC(2 nm)/HAT-CN(7 nm)/Li:Bphen(5 nm)/Bphen(15 nm)/anode and TAPC(2 nm)/HAT-CN(7 nm)/Li:p-bPPhenB(5 nm)/ p-bPPhenB (15 nm). All organic films used for UPS measurements were deposited in a sample preparation chamber that is connected to an analysis chamber, so that samples could be transferred between the chambers without breaking the vacuum. The deposition rate was carefully monitored with a quartz crystal micro-balance and it was typically 0.1 nm/min. We have measured the UPS spectra of organic layers with increasing thickness of deposited layer.

Evaluation of energy level diagrams of CGU interfaces. In the energy level diagrams of Figure 5c and f, HOMO and vacuum levels of each deposited layers are determined by linear extrapolation at the edge of HOMO peak maximum and at the secondary electron cutoff, respectively. the magnitude of band bending is estimated by tracing the HOMO edge shift during the incremental deposition of each layers. The LUMO levels are calculated by subtracting reported charge transporting band gap (4.2 eV for Bphen, 4.1 eV for HATCN and 3.43 eV for TAPC) from HOMO level [1, 2]. In case of p-bPPhenB, charge transporting band gap was estimated using following equation:

$$E_{CTBG\_(B)} \times \frac{E_{OBG\_(p)}}{E_{OBG\_(B)}}$$

Where, $E_{CTBG\_(p)}$, $E_{CTBG\_(B)}$, $E_{OBG\_(p)}$, and $E_{OBG\_(B)}$ represent charge transporting band gap of p-bPPhen, charge transporting band gap of Bphen, optical band gap of p-bPPhen, and optical band gap of Bphen, respectively.

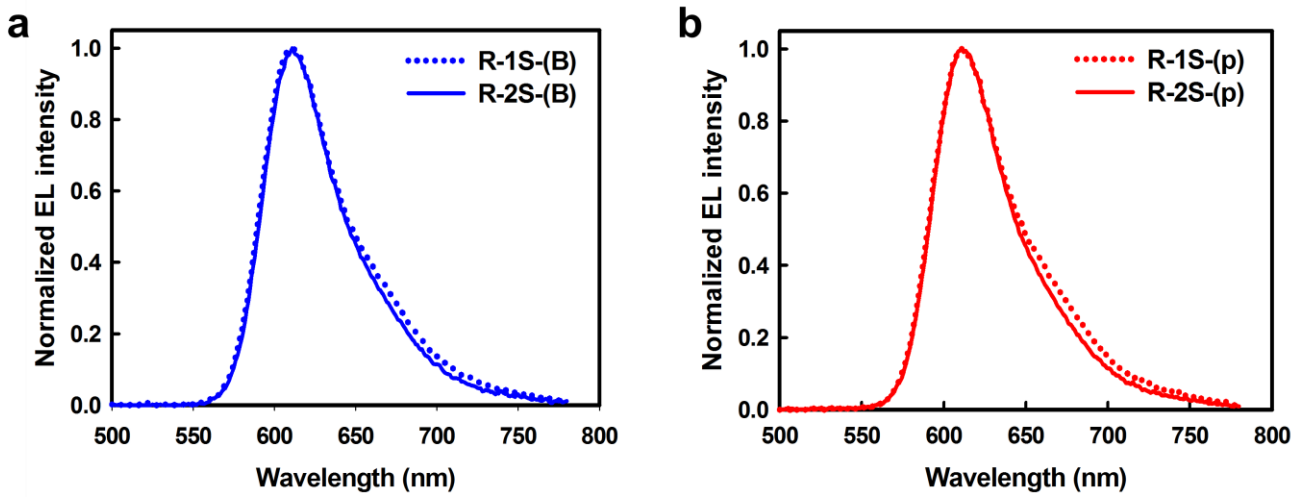

Figure S20. Normalized electroluminescence (EL) spectra of the Bphen (a) and p-bPPhenB (b) based single- and two-stack red PhOLED.

REFERENCES

(1) Meyer, J.; Kröger, M.; Hamwi, S.; Gnam, F.; Riedl, T. *Appl. Phys. Lett.* **2010**, *96*, 193302.
(2) Liu, X.; Yi, S.; Wang, C.; Wang, C.; Gao, Y. *J. Appl. Phys.* **2014**, *115*, 163708.